ELSEVIER

Journal of Organometallic Chemistry 543 (1997) 93–102

Journal of Organometallic Chemistry

Ferrocenylsilatranes
A synthetic, structural and theoretical investigation [1]

Maria J. Calhorda [a], Pedro E.M. Lopes [a], Annette Schier [b], Rudolf Herrmann [c,*]

[a] *Centro de Tecnologia Química e Biológica, R. da Quinta Grande 6, P-2780 Oeiras, Portugal*
[b] *Anorganisch-chemisches Institut der Technischen Universität München, Lichtenbergstr. 4, D-85747 Garching, Germany*
[c] *Institut für Organische Chemie und Biochemie der Technischen Universität München, Lichtenbergstr. 4, D-85747 Garching, Germany*

Received 27 November 1996

Abstract

Ferrocene derivatives containing the silatranyl moiety were prepared and studied by NMR spectroscopy and cyclic voltammetry. Compared with the corresponding triethoxysilanyl derivatives, the silatranes are much more easily oxidized ($\Delta E^{ox}_{1/2}$ up to 0.26 V). In order to understand this result, theoretical calculations (extended Hückel (EH) and density functional theory (DFT)) were performed. The geometries of the four complexes were optimized using DFT calculations. The change in the energy of the HOMO when exchanging $Si(OMe)_3$ for silatranyl as well as the transition state energy using the half-electron approach follow the oxidation potentials. This result can be rationalized from the Si–N anti-bonding character of the HOMO in the silatrane derivatives which leads to an increase in energy. Such a bond is absent in the other species. The prototype of this class of compounds, silatranylferrocene, was characterized by crystal structure analysis. The Si–N distance is 2.181(2) Å and thus lies in the range expected for an aromatic substituent at silicon. The agreement between calculated and observed structure is quite good except for the Si–N distance, where a comparatively large deviation was found which reflects the difference between gas and solid state. A direct interaction between iron and silicon can be excluded for both structural and theoretical reasons. © 1997 Elsevier Science S.A.

1. Introduction

Silatranes (5-aza-2,8,9-trioxa-1-silabicyclo[3.3.3]undecanes) are the most studied class of compounds with hypervalent silicon [1–5]. The nitrogen lone pair donates electrons through space to the d-orbitals of silicon, leading to comparatively high stability of these cage compounds, e.g. towards hydrolysis. A number of silatranes were shown to be highly toxic, while others are of potential pharmacological interest [6]. The combination of the silatrane moiety with organometallics should give an opportunity to study their interactions which can be expected to introduce special properties in the molecules with potential interest for e.g. non-linear optic materials.

This work describes the synthesis and physical properties of derivatives of ferrocene containing the silatranyl moiety, and discusses the interaction between the two parts of the molecules, employing extended Hückel (EH) and density functional theory (DFT) methods. Preliminary results have been presented already [7]. Some ferrocene derivatives with hypervalent silicon, including 1,1′-bis(silatranyl)ferrocene **5**, were also prepared by others [8].

2. Synthesis and properties of silicon derivatives of ferrocene

The synthesis of the silatranes **2**, **5**, and **8** is straightforward and follows normal pathways [2] (Fig. 1). Starting with ferrocene, the triethoxysilylferrocenes **1** and **4** are easily obtained via lithioferrocene [9,10] or 1,1′-dilithioferrocene [11], as well as **7** via the chelate-stabilized lithiated amine obtained from **6** [12] by the reaction with tetraethoxysilane. Transesterification with triethanolamine affords the corresponding silatranes. The conditions (reaction temperature, solvent, catalyst) have to be adjusted for the individual compounds. Silatranyl-

* Corresponding author.

[1] Dedicated to Professor Friedrich Dörr on the occasion of his 75th birthday.

PII S0022-328X(97)00131-9

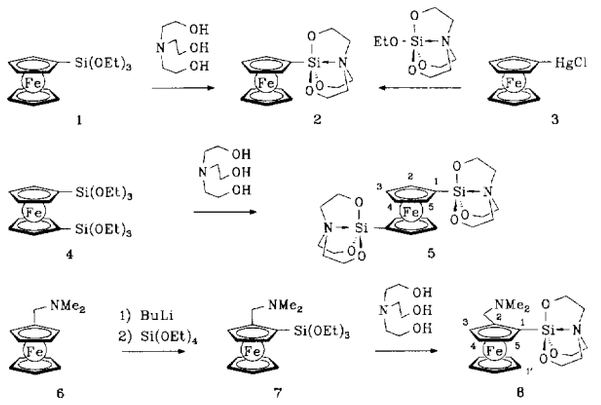

Fig. 1. Synthesis and NMR numbering of silatranylferrocenes.

ferrocene **2** can also be prepared by direct reaction of lithioferrocene (obtained e.g. in situ from chloromercuriferrocene) with ethoxysilatrane, although in comparatively low yield. 1,1′-Dilithioferrocene (as TMEDA complex) [13] and the lithiated amine **6** do not react with ethoxysilatrane, probably because of additional stabilization of the lithium compounds by coordination with nitrogen donors.

The crystal structure analysis (Fig. 2 and Table 1) of silatranylferrocene **2** shows that the ferrocene part of the molecule retains a comparatively undistorted structure; the angle between the planes through the cyclopentadienyl rings is only 3.1°. The fully eclipsed arrangement of these two rings corresponds to that in ruthenocene and in the low-temperature modifications of ferrocene [14,15]. Bond lengths and angles are as expected for a monosubstituted ferrocene derivative. The silatrane moiety retains its non-distorted structure as well. The silicon atom lies in the plane of the attached cyclopentadienyl ring. The distance between iron and silicon atoms is 3.51 Å, which means that there cannot be much direct interaction between these two atoms, although the silicon is in the α-position at ferrocene where such interactions often occur (e.g. in ferrocenylcarbocations). Of particular interest is the silicon–nitrogen distance which was determined as 2.181(2) Å. This weak bond is characteristic for hypervalent silicon compounds [5] and closely resembles the value found in phenylsilatrane (2.193(5) Å in the α-modification [16]). The C1–Si–N angle deviates only slightly from linearity (179.22(8)°), as in most silatranes. Thus, ferrocenyl behaves like a normal aromatic substituent in this respect. This is not surprising in the light of a crystal structure of the compound obtained from phenylsilatrane by coordination of an $Mn(CO)_3$ to the aromatic ring, with almost no influence on the geometry of the silatrane [17].

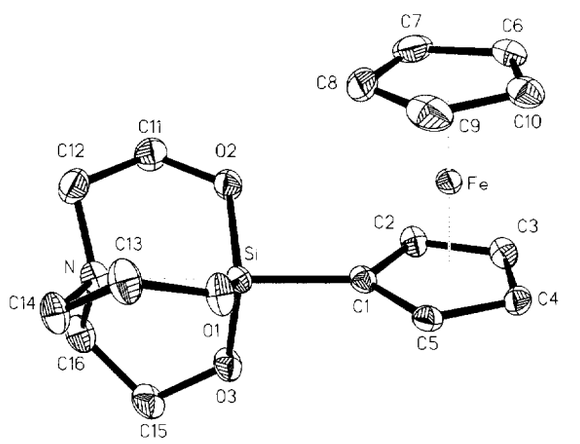

Fig. 2. ORTEP plot (50% probability ellipsoids, H atoms omitted for clarity) of the molecular structure of compound **2**.

Table 1
Crystal structure analysis of **2**. Selected bond lengths and angles

Bond	(Å)	Angle	(°)
Fe–C(1)	2.058(2)	C(1)–Fe–C(8)	103.95(9)
Fe–C(2)	2.042(2)	C(3)–Fe–(C6)	109.67(9)
Fe–C(3)	2.041(2)	O(1)–Si–O(2)	121.07(8)
Fe–C(4)	2.038(2)	O(1)–Si–O(3)	116.92(8)
Fe–C(5)	2.034(2)	O(2 ~ –Si–O(3)	117.47(8)
Si–N	2.181(2)	C(1)–Si–N	179.22(8)
Si–O(1)	1.663(2)	Fe–C(1)–Si	125.84(10)
Si–O(2)	1.660(2)	C(12)–N–C(14)	113.8(2)
Si–O(3)	1.668(2)	C(12)–N–Si	104.74(12)
Si–C(1)	1.877(2)	O(1)–Si–N	83.02(7)

Most chemical shifts in the NMR spectra (^{1}H, ^{13}C, ^{15}N, ^{17}O) lie in the range expected for ferrocenes and silatranes (Table 2); there is not much difference in the behaviour of the triethoxysilane and silatrane moieties. Thus, silatranylferrocene **2** shows a ^{1}H and ^{13}C pattern (^{1}H: 2.86 (t), 3.85 (t, 5.5 Hz); ^{13}C: 50.3 and 57.2 ppm)

Table 2
^{29}Si-, ^{17}O-, and ^{15}N-NMR data, in $CDCl_3$ unless otherwise quoted, and oxidation potentials (Fe(II)–Fe(III) transition) of the compounds **1**, **2**, **4**, **5**, **7**, **8**, and phenyl-silatrane **9**

Compound/ property	δ (^{29}Si)	δ (^{17}O), ($W_{1/2}$ in Hz)	δ (^{15}N)	$E_{1/2}$ (V)
1	−50.9	24 (215)	–	0.03
2	−71.5	20 (540)	22.2	−0.23
4	−50.4 [a]	24 (410)	–	0.11 [b]
5	−71.5 [c]	[d]	[d]	−0.47 [e]
7	−51.7	23 (440)	32.5	0.00
8	−69.6	10 (720)	24.0; 34.2	−0.14
9	−79.8 [f]	20 (330) [g]	24.2 [h]	

[a] [8] gives −47.4 ppm for 1,1′-bis(trimethoxysilyl)ferrocene.
[b] [20] gives 0.07 V for **4**, and [8] gives 0.15 V for 1,1′-bis(trimethoxysilyl)ferrocene.
[c] In $(CD_3)_2SO$; [8] gives −69.69 ppm in $CDCl_3$.
[d] Not determined due to very low solubility in all common NMR solvents.
[e] [8].
[f] [21] gives −81.7 ppm and [22] −80.5 ppm.
[g] [23] gives 21.0 ppm (360 Hz).
[h] [24] gives 22.4 ppm.

similar to phenylsilatrane (^{1}H: 2.79 (t), 3.83 (t, 5.9 Hz); ^{13}C: 50.9 and 57.7 ppm). An empirical correlation between the chemical shifts of the protons of the CH_2N group and the Si–N distance has been suggested [18]: $d(\text{Si–N})/\text{Å} = -\delta/1.21 + 4.51$ ($r = 0.96$).

According to this correlation, the Si–N distance in phenylsilatrane is estimated as 2.20 Å and in silatranylferrocene **2** as 2.15 Å, which is not too far from the experimental values. For the silatranylferrocenes **5** and **8**, where no crystal structures are known, the Si–N distance is predicted from this equation as 2.18 and 2.16 Å respectively, which seems reasonable. A similar correlation has been developed for ^{15}N chemical shifts [19], from which the Si–N distances for **2** and **8** are estimated as 2.20 and 2.17 Å.

The interpretation of ^{29}Si chemical shifts is difficult [3]. It is generally assumed that they decrease on going from lower to higher coordination numbers, i.e. higher coordination implies higher shielding. This is indeed true for the compounds studied here; the triethoxysilylferrocenes **1**, **4**, and **7** (coordination number 4) show chemical shifts between −50.4 and −51.7 ppm while the chemical shifts of the corresponding silatranes (coordination number 5) fall in the range between −69.6 and −71.5 ppm. The shielding effect of a phenyl group towards silicon is more pronounced than that of ferrocene ($\delta = -57.0$ ppm for phenyltriethoxysilane and −79.8 ppm for phenylsilatrane). Considering the high electron donating ability of ferrocene, this seems surprising. The ^{29}Si chemical shift does not, however, only depend on coordination number and electronegativities (σ-donor abilities) of the substituents at silicon, but also on many other factors, e.g. the precise geometry around the silicon atom [3,25]. This is reflected in the O–Si–O bond angles which vary between 116.9 and 121.1° in **2**, but less in phenylsilatrane (117.6–119.6°) [26]. The difference in the chemical shifts between the silane and the silatrane is approximately the same for phenyl and ferrocenyl (~ 20 ppm). This is in accord with an approach which considers diamagnetic terms as opposed to paramagnetic terms in the calculation of the chemical shifts of hypervalent silicon compounds, the balance depending mainly on the Si–N distance [27].

So far, the compounds are not very different from other silatranes with aromatic substituents. However, a dramatic effect is observed on the redox potentials of the transition Fe(II)/Fe(III) (Table 2). The silatranes are much more readily oxidized than the corresponding triethoxysilanes ($\Delta E = 0.26$ V for **1**/**2**). The effect seems to be additive, as the presence of two silatranyl groups doubles the difference in the redox potentials ($\Delta E = 0.58$ V for **4**/**5**). Interestingly, the effect is much less pronounced in the 1,2-disubstituted ferrocene derivatives **7** and **8** ($\Delta E = 0.14$ V). Here, the dimethylamino group could potentially act as an additional ligand for silicon and widen the coordination sphere even more (coordination number 6 in the silatrane). However, there is no convincing evidence for this; if coordination of the dimethylamino occurred one would expect not only different NMR signals for the diastereotopic protons of the adjacent methylene group (which are indeed observed in **7** and **8**), but also for both methyl groups [28] (not observed). Hexacoordination of silicon in a silatrane was found by crystal structure analysis in (8-dimethylamino-1-naphthyl)silatrane [29], but with much longer Si–N distances (2.42 Å in the silatrane moiety and 2.95 Å for the other nitrogen atom). A compound more similar to our case is (2-(1-dimethylamino)ethyl)phenylsilatrane where a lower Si–N distance (2.28 Å) was found in the silatrane moiety and no coordination of the dimethylamino group occurred [29]. Thus, the influence of the dimethylaminomethyl group on the difference of the redox potentials cannot be explained by hexacoordination.

As any ad hoc explanation of the redox potentials (e.g. based on transmission of electron density from nitrogen to iron via silicon) must remain speculative [7,8], a theoretical investigation was required.

3. Molecular orbital calculations

The structures of the four derivatives were optimized using the ADF program [30–32] with a triple ζ basis set for Si, O, N and the adjacent carbon atom (details given in Section 4). The trimethoxysilylferrocenes were studied instead of the triethoxy derivatives to keep the size of the calculation smaller. The dimethylamino group present in two of the compounds was modeled by NH_2. The corresponding model compounds used for the calculations are indicated by a prime, e.g. 2-aminomethyl-1-trimethoxysilylferrocene **7'** is the model for compound **7**. The structures are drawn in Fig. 3 and relevant bond distances and angles are collected in Table 3.

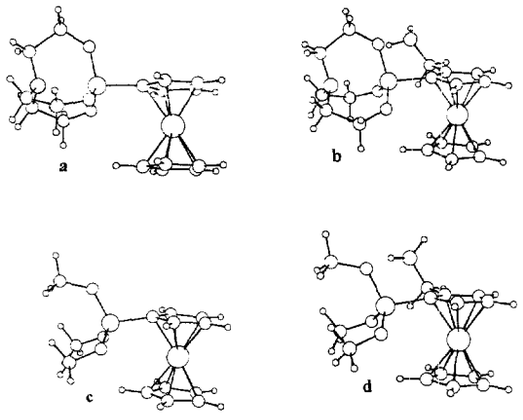

Fig. 3. Optimized geometries (DFT, method A) of the compounds **2** (upper left), **1'** (lower left), **8'** (upper right), and **7'** (lower right).

Table 3
Optimized geometries for **2**, **8′**, **1′**, and **7′** (relevant distances (Å) and angles (°))

Bond, angle/compound	2	8′	1′	7′
Fe–Cl	2.034	2.033	2.033	2.036
Si–N	2.386	2.442	–	–
Si–O	1.649	1.648	1.639	1.642
Si–Cl	1.845	1.846	1.808	1.813
C–C(NH_2)	–	1.496	–	1.492
C(NH2)–N	–	1.444	–	1.449
Cl–Fe–C8	107.50	105.84	107.46	109.66
C3–Fe–C6	108.6	107.51	108.04	107.88
O–Si–O	116.92	116.11	111.13	110.74
Fe–Cl–Si	125.37	121.56	112.84	114.95
C12–N–Si	103.52	102.92	–	–

It can be seen that the agreement between the calculated and experimental distances (compound **2**) and angles is very satisfactory. As the four compounds belong to the same family it is expected that the calculated geometries for the other three will also be good approximations. The major exception refers to the Si–N bond, one of the most typical features of silatranes, which comes too long in the calculations. In order to estimate the influence of basis set on this distance, the geometries of **2** were optimized in different conditions (Table 4; see Section 4 for details).

A is the basis set used to optimize the geometries of the four species, as referred to above. In **B**, a smaller basis set was used (double ζ), while in **C** a polarization function was added to the basis set of **A**. While most bond distances and angles do not vary significantly with the basis set, the Si–N distance decreases, getting closer to the experimental value. Thus it is particularly this weak bond which is sensitive to modifications of the basis sets. Similar observations were made earlier by Gordon and coworkers who did calculations at the RHF/6-31G(d) level for a series of small atranes [33,34]. They observed even larger discrepancies between calculated and experimental Si–N distances (both X-ray and gas phase results) and realized that this bond could be very easily distorted by packing forces in a crystal. Indeed, when the structures in the gas and solid state are known, it is seen that this bond varies significantly. For the fluorosilatrane, it shrinks from 2.324 to 2.042 Å when going from the gas to the solid state [35]. Considering that our calculations reproduce the behavior of the molecule in the gas phase, it is not surprising that the predicted value is longer than the one found in the crystal structure. The good overall agreement in calculated and observed structural parameters allows us to rely upon the quality of the optimized geometry for the three remaining compounds. In **7′** and **8′**, the distance between the silicon atom and the nitrogen atom of the NH_2 group (> 3.4 Å in both compounds) exceeds considerably the Si–N distance in the silatrane. The nitrogen atom has a pyramidal structure which means that it does not interact with silicon to form a hexacoordinated species.

Table 4
Optimized geometries of **2** using different basis sets **A**, **B**, and **C** (relevant distances (Å) and angles (°))

Bond, angle/method	A	B	C	Crystal structure
Fe–Cl	2.034	2.026	2.029	2.034–2.058
Si–N	2.386	2.360	2.276	2.181
Si–O	1.649	1.650	1.674	1.660–1.668
Si–Cl	1.845	1.848	1.854	1.877
Cl–Fe–C8	107.50	107.56	107.78	103.95
C3–Fe–C6	108.06	108.33	108.42	109.67
O–Si–O	116.92	117.12	117.90	116.92–121.07
Fe–Cl–Si	125.37	125.94	126.38	125.84
C12–N–Si	103.52	103.94	105.47	104.74
O–Si–N	79.88	80.22	81.69	82.48–83.15

Optimizing the geometry of the four compounds was the first step in trying to understand the change observed in their oxidation potentials. The simplest and crudest approach is to consider that the energy of the HOMO parallels the oxidation potentials [36]: the higher the HOMO energy, the lower the oxidation potential. This can be done in both EH and DFT calculations. A better way to determine the ionization energy, incorporating electron relaxation effects, is to calculate the difference between the energies of the cation and the neutral molecule [37]. Problems of achieving convergence in optimizing the ions prevented us from using this approach. Another method used for this purpose is the transition state method, in which the orbital occupancy of the initial neutral species has been decreased by one half electron [38,39]. The results are shown in Table 5.

The largest effect on the redox potentials is observed when the trimethoxysilyl moiety is replaced by the silatrane, while the introduction of the side chain, CH_2NH_2, has a much less pronounced effect. Experimentally, the side chain leads to an increase of half wave potential for the silatrane derivative **8** and has the opposite effect on the trimethoxysilyl compound **7**. This observation is reproduced by the change in the HOMO energy (ADF), but not by the transition state method. Maybe the fact that the orientation of the side chain is very sensitive to the method of calculation plays a role

Table 5
Calculated HOMO energies and transition state energies (eV) for compounds **1′**, **2**, **7′**, and **8′**, and experimental oxidation potentials ($E^{ox}_{1/2}$, V) for **1**, **2**, **7**, and **8**

Compund/ method	HOMO (ADF)	HOMO (EH)	TS	$E^{ox}_{1/2}$
2	4.009	−11.62	7.413	−0.23
8′/8	4.012	–	7.366	−0.14
1′/1	4.554	−11.82	7.874	0.03
7′/7	4.464	–	7.766	0.00

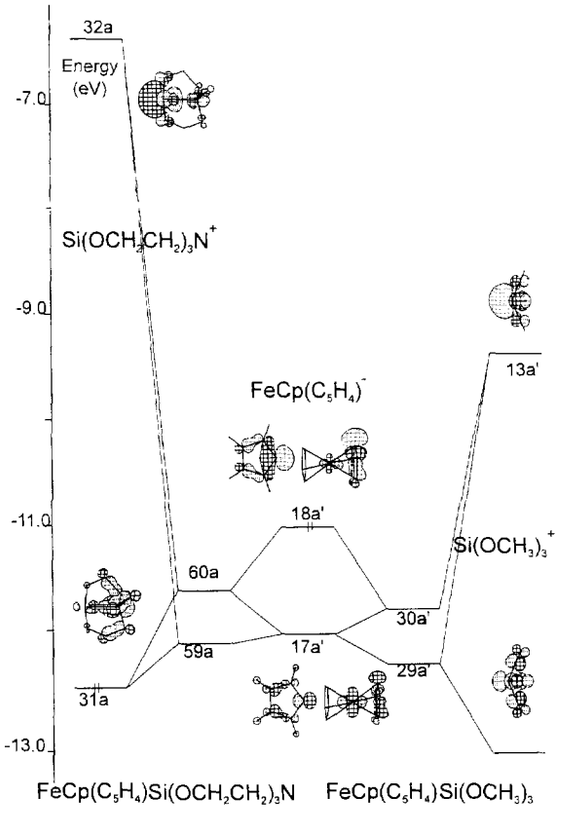

Fig. 4. Simplified diagram showing the interaction between $Fe(C_5H_5)(C_5H_4)^-$, and $Si(OCH_2CH_2)_3N^+$ (left side) or $Si(OMe)_3^+$ (right side).

here. In solution the situation is probably different and the outcome may consequently vary.

Taking into account these results, only an explanation of the major effect, reproduced by all types of calculations, will be attempted. We start by looking at the results of the extended Hückel calculations, because they allow us to trace the origin of the shift in the energy of the HOMO more easily. Fig. 4 represents part of an interaction diagram between the ferrocenyl anion, $Fe(C_5H_5)(C_5H_4)^-$, and the silatranyl (left side) or trimethoxysilyl cation (right side) to form the C–Si bond. The metal fragment acts as donor through the carbon lone pair (shown in the center of the diagram in two views), while the acceptor orbital is mainly a lone pair at silicon. The low symmetry of the compounds allows many mixings of orbitals, which makes the diagram more complicated. However, the main difference between the two silicon fragments is the higher energy of the LUMO (32a, left) of the silatrane which gives rise to a higher energy HOMO (60a) of the final molecule **2** when compared to the $Si(OMe)_3^+$ fragment (LUMO 13a′, right) and its ferrocenyl derivative **1′** (HOMO 30a′). The higher energy LUMO of the silatrane is in turn caused by the Si–N anti-bonding nature of that orbital, something which cannot be present in the $Si(OR)_3$ fragments, where neither nitrogen nor any other atom in the same situation exists and the LUMO is almost non-bonding.

It is difficult to directly compare the previous interpretation with what can be extracted from the DFT calculations. The same two molecules (**1′** and **2**) were decomposed in two fragments, the $Fe(C_5H_5)(C_5H_4)$ radical and the silatranyl or trimethoxysilyl radical. These two fragments interact to form a C–Si bond. The half-filled HOMO of the metallic fragment can be described as essentially a carbon lone pair mostly located

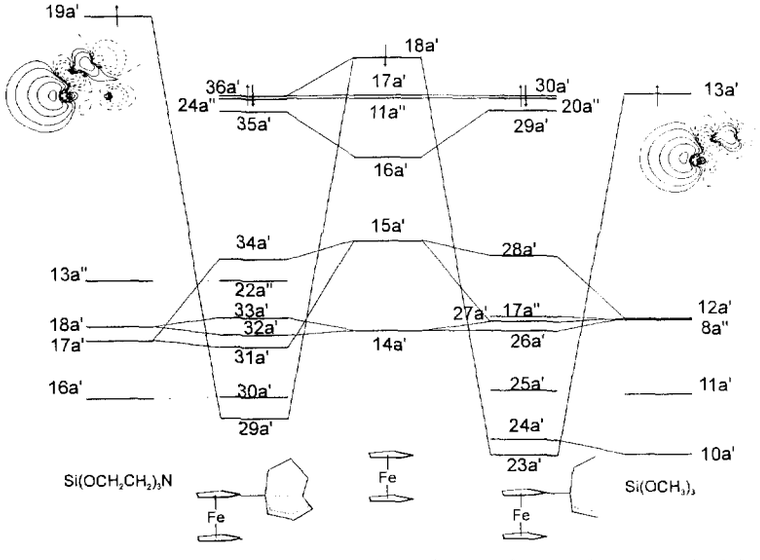

Fig. 5. Schematic diagram showing the interaction between $Fe(C_5H_5)(C_5H_4)$ (center) and $Si(OCH_2CH_2)_3N$ (left) or $Si(OMe)_3$ (right) radicals and the HOMOs of the silicon containing fragments. In the wavefunction plots, solid and dashed lines represent positive and negative amplitudes, respectively, and the node is the dotted–dashed line. Contours are 0.01, 0.02, 0.05, 0.1, 0.2, and 0.5 $e*bohr^{-3}$.

at the carbon atom forming the new bond, and in the iron atom. There are many other orbitals sharing the carbon lone pair character, owing to the low symmetry of the fragment. The HOMOs of the two silicon containing fragments differ considerably, in the same way as observed above; in the silatrane, this orbital exhibits a large Si–N anti-bonding character which is missing in $Si(OMe)_3$. $Fe(C_5H_5)(C_5H_4)$ and each of the other two fragments interact as depicted in Fig. 5. The relative energy scale between fragments and molecules was adjusted according to Mulliken contributions of fragment orbitals [40] to visualize the interactions in an easier way. This adjustment puts the HOMOs of the two ferrocene derivatives at the same energy.

The most striking feature of this diagram is the considerable mixing of all orbitals having the same symmetry (either a′ or a″). The HOMO is an a′ orbital as well as the orbital representing the Si–C bond. Table 6 gives the composition of the most relevant molecular orbitals as a function of the fragment orbitals, and it can easily be seen how all the a′ fragment orbitals mix. The strongest interaction leads to MOs 29a′ (left) and 24a′ (right), which are shown in Fig. 6, along with the HOMOs (36a′ and 30a′) of the two molecules.

We can notice that some Si–C character has appeared in the HOMOs owing to mixing between orbitals of the same symmetry. The fact that the Si–N antibonding silatrane HOMO has a higher energy is reflected in the higher energy of the MOs deriving from it, as can be seen when comparing the left and right sides of the diagram in Fig. 5. Therefore, although not so evident, it seems that the high energy HOMO of the silatrane derivative can be traced to similar reasons by the two methods.

Table 6
Composition of the more relevant molecular orbitals of 2′ and 1′ as a function of fragment orbitals

2	Ferrocenyl	Silatranyl	1	Ferrocenyl	Trimethoxysilyl
MO	Composition (%)		MO	Composition (%)	
36a′	9 (16a′)		20a″	99 (11a″)	
	76 (17a′)				
	14 (18a′)				
24a″	100 (11a″)		30a′	3 (16a′)	
				84 (17a′)	
				11 (18a′)	
35a′	56 (16a′)		29a′	61 (16a′)	
	22 (17a′)			12 (17a′)	
	21 (18a′)			25 (18a′)	
34a′	88 (15a′)	10 (17a′)	28a′	76 (15a′)	18 (12a′)
23a″	98 (10a′)		19a″	19 (10a″)	80 (9a″)
22a″		98 (13a″)	18a″	79 (10a″)	19 (9a″)
33a′	63 (14a′)	12 (18a′)	17a″		98 (8a″)
	81 (18a′)	5 (19a′)			
21a″	99 (9a″)		27a′	10 (14a′)	76 (12a′)
				10 (15a′)	
32a′	14 (14a′)	84 (18a′)	16a″	98 (9a″)	
20a″		99 (12a″)	26a′	75 (14a′)	5 (12a′)
				9 (15a′)	
				5 (16a′)	
31a′	8 (15a′)	87 (17a′)	25a′		94 (11a′)
30a′		86 (16a′)	15a″		98 (7a″)
19a″		99 (11a″)	24a′	4 (14a′)	47 (10a′)l
				8 (16a′)	16 (13a′)
				12 (18a′)	
29a′	17 (14a′)	9 (15a′)	23a′	5 (14a′)	50 (10a′)
	11 (16a′)	13 (16a′)		9 (16a′)	10 (13a′)
	16 (18a′)	19 (19a′)		12 (18a′)	

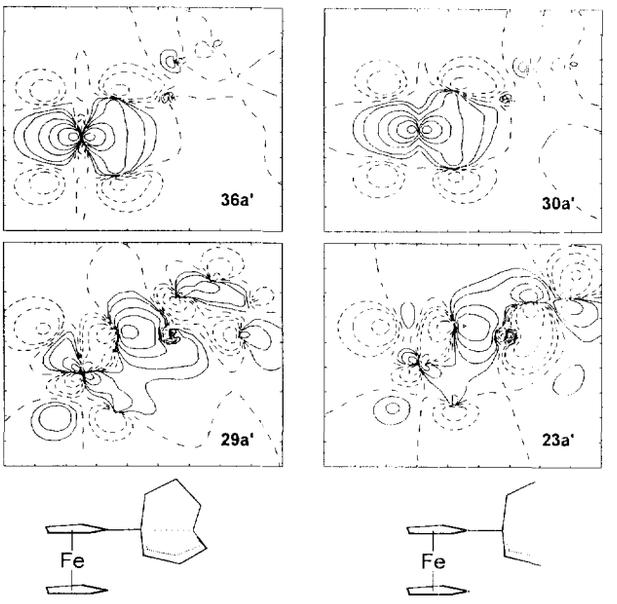

Fig. 6. Some relevant molecular orbitals of **1′** and **2**. In the wavefunction plots, solid and dashed lines represent positive and negative amplitudes, respectively, and the node is the dotted–dashed line. Contours are 0.01, 0.02, 0.05, 0.1, 0.2, and 0.5 $e * \text{bohr}^{-3}$.

4. Experimental

4.1. General

NMR spectra were measured with a Bruker AM 360 instrument (360.134 MHz for ^{1}H, 90.556 MHz for ^{13}C, 71.544 MHz for ^{29}Si, 48.850 MHz for ^{17}O and 36.492 MHz for ^{15}N). For NMR numbering of the carbon atoms, see Fig. 1. ^{1}H, ^{13}C, and ^{29}Si spectra were calibrated relative to internal TMS. ^{17}O NMR spectra were obtained at 50 °C, using the pulse sequence of Goc and Fiat [41] for the suppression of acoustic ringing. All other spectra were obtained at room temperature. Inverse gated decoupling was used for the detection of ^{29}Si and ^{15}N, with 1% $Cr(acac)_3$ added. ^{15}N spectra were calibrated relative to external 50% nitromethane in $CDCl_3$ ($\delta = 379.6$ ppm) and ^{17}O spectra relative to external H_2O ($\delta = 0$ ppm). Electrochemical studies were performed with an EG&G PAR 173 potentiostat and an EG&G PARC 175 universal programmer, using a 0.2

molar solution of NBu_4BF_4 in THF, a platinum working electrode, and a silver reference electrode. Potentials were determined relative to the internal cyanoferrocene/cyanoferrocinium redox couple ($E^{ox}_{1/2} = 0.89$ V vs. SCE) [42]. They are quoted relative to ferrocene/ferrocinium ($E^{ox}_{1/2} = 0$V). Mass spectra were obtained with a Varian MAT CH5 spectrometer (70 eV).

4.2. Crystal structure determination of 2

An orange crystal of **2** ($C_{16}H_{21}FeNO_3Si$, M_r = 359.28 amu) showed the monoclinic space group $P2_1/c$, with the unit cell dimensions $a = 6.744(2)$, $b = 10.128(1)$, $c = 22.141(4)$ Å; $\beta = 93.37(3)°$; $Z = 4$, $V = 1509.7(5)$ Å^3, $\rho_{calc} = 1.581$ g cm^{-3}, $F(000) = 752$. Mo Kα radiation ($\lambda = 0.71073$ Å) was used.

The data collection was performed with a CAD4 (Enraf–Nonius) diffractometer with a graphite monochromator, at 205 ± 2 K, in the range $3.03° < \Theta < 25.93°$ (h −8/+8, k 0/12, l 0/27). Data were corrected for Lorentz and polarization effects as well for absorption (ψ-scans, $T_{min}/T_{max} = 0.95/0.99$; μ(Mo Kα) = 10.9 mm^{-1}. 2840 reflections were collected, and 2775 independent reflections ($R_{int} = 0.0161$) were used for the structure determination by full-matrix least-squares refinement on F^2. 283 parameters were full-matrix refined. In the last refinement step, convergence was achieved with $R_1 = 0.0262$, $wR_2 = 0.0668$ ($I > 2\sigma(I)$); GOOF = 1.079. The residual electron density was +0.371 e Å^{-3}/−0.515 e Å^{-3}. Further information on the crystal structure determination can be obtained from Fachinformationszentrum Karlsruhe, D-76344 Eggenstein-Leopoldshafen, on quoting the CSD-number 406097.

4.3. Synthesis of the compounds

4.3.1. Triethoxysilylferrocene 1

A solution of bromoferrocene (2.31 g, 8.7 mmol) in dry diethyl ether (80 ml) was cooled to −40 °C under N_2, and butyllithium (8.7 mmol, 3.5 ml of 2.5 M hexane solution) was added dropwise with stirring. After 20 min a solution of tetraethoxysilane (1.88 g, 9 mmol) in dry diethyl ether (20 ml) was added dropwise. The mixture was allowed to come to room temperature and stirred for 12 h. The solids were filtered off and washed carefully with dry diethyl ether. The solvents were removed in vacuum from the combined solutions. **1** was obtained as a dark red oil, which hydrolyzes too fast for microanalysis and mass spectroscopy. Yield 2.43 g (80%). ^{1}H NMR ($CDCl_3$): 1.27 (t, 9 H, 7.0 Hz), 3.93 (qua, 6 H, 7.0 Hz), 4.21 (s, 5 H), 4.24 (t, 2 H, 1.8 Hz), 4.35 (t, 2 H, 1.8 Hz). ^{13}C NMR ($CDCl_3$): 61.8 (C-1), 70.8, 73.4 (C-2–C-5), 68.6 (C-1′), 58.4 (CH_2), 18.3 (CH_3). ^{1}H NMR (C_6D_6): 1.21 (t, 3 H, 6.4 Hz), 3.89 (qua, 2 H, 6.4 Hz), 4.21 (s, 5 H), 4.24 (m, 2 H), 4.29 (m, 2 H). ^{13}C NMR (C_6D_6): 62.5 (C-1), 71.3, 74.0 (C-2–C-5), 69.3 (C-1′), 58.7 (CH_2), 18.6 (CH_3).

4.3.2. Silatranylferrocene 2

(a) From triethoxysilylferrocene **1**. Finely powdered lithium hydroxide (0.30 g, 11.5 mmol) was suspended by vivid stirring in xylene (80 ml) under N_2. Triethanolamine (1.10 g, 7.4 mmol) and **1** (2.40 g, 7.0 mmol) were added, and a distillation head was connected to the flask. The temperature of the heating bath was raised to 135 °C for 21 h, during which time 1.2 ml of ethanol (100%) distilled. After cooling to room temperature, the mixture was filtered and the remaining solid washed with $CHCl_3$ (5 × 50 ml). The solvents were removed in vacuum from the combined organic solutions, and the residue was purified by chromatography (silicagel, first CH_2Cl_2 to remove the impurities, then ethyl acetate; R_f (CH_2Cl_2) 0.11, (ethyl acetate) 0.44). Crystals suitable for crystal structure analysis were grown from acetone. Yield 1.50 g (60%), m.p. 255–260 °C (dec.). ^{1}H NMR ($CDCl_3$): 2.86 (t, 6 H, 5.5 Hz, CH_2N), 3.85 (t, 6 H, 5.5 Hz, CH_2O), 4.13 (s, 5 H), 4.16 (t, 2 H, 1.9 Hz), 4.18 (t, 2 H, 1.9 Hz). ^{13}C NMR ($CDCl_3$): C-1 not detected, 69.7, 73.7 (C-2–C-5), 68.4 (C1′), 51.1 (CH_2N), 58.1 (CH_2O). ^{1}H NMR (C_6D_6/$(CD_3)_2$SO 1:1): 2.61 (t, 6 H, 5.9 Hz), 3.67 (t, 6 H, 5.9 Hz), 4.18 (s, br, 2 H), 4.22 (s, 5 H), 4.34 (s, br, 2 H). ^{13}C NMR (C_6D_6/$(CD_3)_2$SO 1:1): 76.2 (C-1), 68.6, 73.9 (C-2–C-5), 68.2 (C-1′), 50.3 (CH_2N), 57.2 (CH_2O). Mass spectrum: m/z 359 (M^+), 174 (silatranyl$^+$), 121 (cpFe$^+$). Anal. Found: C, 53.7; H, 6.2; N, 3.7. $C_{16}H_{21}FeNO_3Si$ Calc.: C, 53.5; H, 5.9; N, 3.9%.

(b) From chloromercuriferrocene **3**. To a suspension of **3** (3.36 g, 8.0 mmol) in dry diethyl ether (50 ml) was added dropwise under N_2 butyllithium (16 mmol, 6.4 ml of 2.5 M hexane solution). After stirring for 1 h, ethoxysilatran [2] (2.63 g, 12 mmol) was added and the mixture stirred for 12 h at room temperature and then 1 h under reflux. After cooling to room temperature, the solids were filtered off and washed with $CHCl_3$ (5 × 50 ml). The solvents were removed in vacuum from the combined solutions, and the residue was purified by chromatography as above, yielding 0.46 g (16%) of **2**.

4.3.3. 1,1′-Bis(triethoxysilyl)ferrocene 4

The compound was prepared in analogy to 1,1′-bis(trimethoxysilyl)ferrocene [8], by replacing chlorotrimethoxysilane by tetraethoxysilane, yield 64% of a dark red oil. ^{1}H NMR: 1.28 (t, 18 H, 7.0 Hz), 3.93 (qua, 12 H, 7.0 Hz), 4.25 (t, 4 H, 1.5 Hz), 4.45 (t, 4 H, 1.5 Hz). Ref. [20] gives 1.02 (t), 3,93 (qua), 4.39 (t), 4.63 (t) in C_6D_6. ^{13}C NMR: 68.8 (C-1), 72.2, 74.0 (C-2–C-5), 58.6 (CH_2), 18.3 (CH_3).

4.3.4. 1,1'-Bis(silatranyl)ferrocene 5

This compound was prepared as described [8]. ^{1}H NMR ($(CD_3)_2SO$): 2.82 (t, 12 H, 5.9 Hz, CH_2N), 3.68 (t, 12 H, 5.9 Hz, CH_2O), 3.88 (s, br, 4 H), 3.95 (s, br, 4 H). Ref. [8] gives 2.69 (m, 12 H), 3.71 (m, 12 H), 3.92–4.32 (m, 8 H) in $CDCl_3$. ^{13}C NMR ($(CD_3)_2SO$): 74.3 (C-1), 70.1, 73.4 (C-2–C-5), 50.5 (CH_2N), 57.3 (CH_2O). Ref. [8] gives 71.8 (C-1), 74.2, 77.6 (C-2–C-5), 52.0 (CH_2N), 58.7 (CH_2O) in $CDCl_3$.

4.3.5. 2-(N,N-Dimethylaminomethyl)-1-triethoxysilylferrocene 7

To a solution of *N,N*-dimethylaminomethylferrocene **6** (1.22 g, 5.0 mmol) in dry diethyl ether (20 ml) was added butyllithium (5.0 mmol, 2.0 ml of 2.5 M hexane solution) dropwise under N_2. The mixture was refluxed for 16 h. At room temperature, tetraethoxysilane (5.0 ml) was added and the mixture refluxed for 4 h. After cooling to room temperature, the solids were filtered off and washed with diethyl ether (3 × 30 ml). The solvents and excess tetraethoxysilane were removed in vacuum from the combined solutions. From the residue, unreacted **6** was removed by bulb-to-bulb distillation (0.1 torr, 150 °C bath temperature). The product was a viscous red oil, yield 1.50 g (74%) which hydrolyzes too fast for mass spectroscopy and microanalysis. ^{1}H NMR ($CDCl_3$): 1.26 (t, 9 H, 6.8 Hz), 2.15 (s, 6 H), 3.91 (qua, 6 H, 6.8 Hz), 3.18 and 3.52 (two d, 1 H each, 12.3 Hz, CH_2N), 4.12 (s, 5 H), 4.18 (s, br, 1 H), 4.24 (s, br, 1 H), 4.34 (s, br, 1 H). ^{13}C NMR ($CDCl_3$): 62.8 (C-1), 89.6 (C-2), 70.4, 73.3, 74.6 (C-3–C-5), 69.4 (C-1'), 58.5 (CH_2N), 58.4 (CH_2O), 44.8 (CH_3N), 18.2 (CH_3CH_2O). ^{1}H NMR (C_6D_6): 1.23 (t, 9 H, 6.5 Hz), 2.15 (s, 6 H), 2.98 and 3.81 (two d, 1 H each, 12.1 Hz, CH_2N), 3.97 (qua, 6 H, 6.5), 4.09 (s, br, 1 H), 4.19 (s, 5 H), 4.30 (s, br, 2 H). ^{13}C NMR (C_6D_6): 63.6 (C-1), 91.1 (C-2), 70.8, 74.5, 75.8 (C-3–C-5), 70.2 (C-1'), 59.7 (CH_2N), 59.1 (CH_2O), 45.6 (CH_3N), 19.1 (CH_3CH_2O).

4.3.6. 2-(N,N-Dimethylaminomethyl)-1-silatranylferrocene 8

To a solution of **7** (0.81 g, 2.0 mmol) and triethanolamine (0.30 g, 2.0 mmol) in toluene (25 ml) was added under N_2 finely powdered LiOH (30 mg, 1.2 mmol). A distillation head was connected to the flask, and the mixture was heated to 150 °C (bath temperature) for 2.5 h during which time 0.8 ml of distillate was collected. After cooling to room temperature, the solids were filtered off and the residue washed with CH_2Cl_2 (3 × 20 ml). The solvent was removed in vacuum from the combined solutions, and the residue was purified by chromatography (neutral alumina, $CHCl_3/HNEt_2$ 20:1, R_f 0.85). The oily residue obtained after the evaporation of the solvent was extracted with hexane (10 ml), upon which treatment it turned into a waxy solid, yield 0.50 g (60%), m.p. 105–109 °C. ^{1}H NMR ($CDCl_3$): 2.24 (s, 6 H, CH_3N), 2.84 (t, 6 H, 5.7 Hz, CH_2NCH_2), 3.82 (t, 6 H, 5.7 Hz, CH_2O), 3.43 and 3.68 (two d, 1 H each, 13.1 Hz, CH_2NCH_3), 4.05 (s, 5 H), 4.15, 4.17 (two s, 1 H each, H-4, H-5), 4.25 (s, 1 H, H-3). ^{13}C NMR ($CDCl_3$): 73.3 (C-1), 87.6 (C-2), 72.3 (C-3), 69.6, 74.9 (C-4, C-5), 69.0 (C-1'), 51.8 (CH_2NCH_2), 58.5 (CH_2NCH_3), 58.3 (CH_2O), 44.7 (CH_3N). Mass spectrum: *m/z* 416 (M^+), 372 ($M-NMe_2^+$), 174 (silatranyl$^+$). Anal. Found: C, 55.1, H, 6.9; N, 6.7. $C_{19}H_{28}FeN_2O_3Si$. Calc.: C, 54.8, H, 6.8, N, 6.7%.

4.4. Calculations

The DFT calculations reported in this paper are based on the Amsterdam DF program package (ADF) [30–32,43,44] characterized by the use of a density fitting procedure [30–32] to obtain accurate Coulomb and exchange potentials in each SCF cycle, by accurate and efficient numerical integration [43,44] of the effective one-electron Hamiltonian matrix elements and by the possibility of freezing core orbitals [30].

The LSD exchange potential and energy were used [45], together with the Vosko–Wilk–Nusair [46] parametrization for homogeneous electron gas correlation, including Stoll's correction for correlation between electrons of different spin [47]. The production basis set (referenced in text as **A**) consisted of an uncontracted triple ζ STO basis augmented with polarization functions for silicon and neighboring atoms: oxygen, nitrogen and carbon in the substituted cyclopentadienyl ring. The orbitals for iron consisted in an expansion of a triple ζ STO basis set. The orbitals of hydrogen and the remaining carbon atoms in the cyclopentadienyl rings consisted in an expansion of a double ζ STO basis set and that of the carbons and hydrogens in the silatrane and trimethoxysilane in an expansion of a double ζ STO basis set augmented with polarization functions. The effect of basis sets on the molecular structure was studied considering two other expansions: **B** consisting of a triple ζ STO basis augmented with polarization functions for all atoms except carbon and hydrogen expanded in a double ζ STO basis and iron kept with a triple ζ STO expansion, and **C** consisting of a double ζ STO basis augmented with polarization functions for all atoms except iron where we used a triple ζ expansion.

The geometries were optimized using gradient techniques [48]. The symmetry was kept as high as possible, namely C_s for the silatrane and trimethoxysilane derivatives and C_1 for the substituted analogues. Considering the size of the molecules, a full optimization was not done. The ferrocenyl fragment was frozen, only the cyclopentadienyl (centroid)–Fe–cyclopentadienyl (centroid) unit being allowed to change. The silicon containing fragments (silatrane and trimethoxysilane)

were fully optimized, as well as their orientation relative to the attached cyclopentadienyl ring. The side chain, modeled as CH_2NH_2, was fully optimized except for the C–H and N–H distances which were kept constant.

The calculations using the extended Hückel (EH) method [49–51] were done with modified H_{ij}s [52] with the CACAO programme [53]. Only s and p orbitals were used for silicon. The s and p orbitals were described by single Slater-type wave functions, and the d orbitals were taken as contracted linear combinations of two Slater-type wave functions. Standard parameters were used for H, C, O, N and Si, and the following for Fe (H_{ii}/eV, ζ): 4s −9.17, 1.900; 4p −5.37, 1.900; 3d, −12.70, 5.35, ζ_2 1.80, C_1 0.5366, C_2 0.6678.

Idealized models for the silatrane and trimethoxysilane derivatives of C_s symmetry were used. The cyclopentadienyl rings were kept eclipsed and parallel. The following distances (Å) were used: Fe–cyclopentadienyl (centroid) 1.660, C(cyclopentadienyl)–Si 1.900, Si–O 1.660, O–C 1.42, C–C 1.540 and Si–N 2.130.

Acknowledgements

We wish to thank Professor Dr. Ivar Ugi, TU München, for supporting this work, Professor Dr. Fernanda N.N. Carvalho, Instituto Superior Técnico, Lisboa, Portugal for her help in electrochemical measurements, and Mr. J. Riede for establishing the crystallographic data. We thank Gabriele Wagner, Roland Fischer, Richard Fischer, Park Seyong-Yon and Thomas Probst for performing some experiments. We also acknowledge JNICT for a grant to P.E.M. Lopes and the European Community, Human Capital and Mobility programme for a grant to M.J. Calhorda and P.E.M. Lopes.

References

[1] M.G. Voronkov, Pure Appl. Chem. 13 (1966) 35.
[2] M.G. Voronkov, V.M. Dyakov, S.V. Kirpichenko, J. Organomet. Chem. 233 (1982) 1.
[3] S.N. Tandura, M.G. Voronkov, N.V. Alekseev, Top. Curr. Chem. 131 (1986) 99.
[4] V.E. Shklover, Y.T. Struchkov, M.G. Voronkov, Usp. Khim. 58 (1989) 353 (Engl. p. 211).
[5] R.J.P. Corriu, J. Organomet. Chem. 400 (1990) 81.
[6] M.G. Voronkov, Top. Curr. Chem. 84 (1979) 77.
[7] R. Herrmann, XIV Int. Conf. on Organometallic Chemistry (ICOC), Torino, 1988 (Conf. Abstr. 134).
[8] G. Cerveau, C. Chuit, E. Colomer, R.J.P. Corriu, C. Reyé, Organometallics 9 (1990) 2415.
[9] R.W. Fish, M. Rosenblum, J. Org. Chem. 30 (1965) 1253.
[10] D. Guillaneux, H.B. Kagan, J. Org. Chem. 60 (1995) 2502.
[11] J.J. Bishop, A. Davison, M.L. Katcher, D.W. Lichtenberg, R.E. Merrill, J.C. Smart, J. Organomet. Chem. 27 (1971) 241.
[12] D.W. Slocum, B.W. Rockett, C.R. Hauser, J. Am. Chem. Soc. 87 (1965) 1241.
[13] M.D. Rausch, D.J. Ciappenelli, J. Organomet. Chem. 10 (1967) 127.
[14] J.-F. Bérar, G. Calvarin, D. Weigel, K. Chhlor, C. Pommier, J. Chem. Phys. 73 (1980) 438.
[15] P. Seiler, J.D. Dunitz, Acta Crystallogr. 38b (1982) 1741.
[16] L. Párkányi, K. Simon, J. Nagy, Acta Crystallogr. 30b (1974) 2328.
[17] Y.-A. Lee, Y.K. Chung, Y. Kim, J.H. Jeong, Organometallics 9 (1990) 2851.
[18] S.N. Tandura, V.A. Pestunovich, G.I. Zelchan, V.P. Baryshok, Y.A. Lukina, M.S. Sorokin, M.G. Voronkov, Izv. Akad. Nauk SSSR, Ser. Khim. (1981) 295 (Engl. p. 223).
[19] V.A. Pestunovich, B.Z. Shterenberg, É.T. Lippmaa, M.Y. Myagi, M.A. Alla, S.N. Tandura, V.P. Baryshok, L.P. Petukhov, M.G. Voronkov, Dokl. Akad. Nauk SSSR 258 (1981) 1410.
[20] M.S. Wrighton, M.C. Palazzotto, A.B. Bocarsly, J.M. Bolts, A.B. Fischer, L. Nadjo, J. Am. Chem. Soc. 100 (1978) 7264.
[21] R. Harris, J. Jones, Hg. Soon, J. Magn. Res. 30 (1978) 521.
[22] V.A. Pestunovich, S.N. Tandura, M.G. Voronkov, G. Engelhardt, E. Lippmaa, T. Pekh, V.F. Sidorkin, G.I. Zelchan, V.P. Baryshok, Dokl. Akad. Nauk SSSR 240 (1978) 914.
[23] É.É. Liepin'sh, I.A. Zitzmane, G.I. Zelchan, É. Lukevits, Zh. Obsh. Khim. 53 (1983) 245 (Engl. p. 215).
[24] É.L. Kupche, É. Lukevits, Khim. Geterot. Soed. 5 (1989) 701 (Engl. p. 586).
[25] J.H. Iwamiya, G.E. Maciel, J. Am. Chem. Soc. 115 (1993) 6835.
[26] L. Párkányi, J. Nagy, K. Simon, J. Organomet. Chem. 101 (1975) 11.
[27] V.F. Sidorkin, V.A. Pestunovich, M.G. Voronkov, Magn. Res. Chem. 23 (1985) 491.
[28] F. Carré, R.J.P. Corriu, A. Kpoton, M. Poirier, G. Royo, J.C. Young, C. Belin, J. Organomet. Chem. 470 (1994) 43.
[29] F. Carré, G. Cerveau, C. Chuit, R.J.P. Corriu, N.K. Nayyar, C. Reyé, Organometallics 9 (1990) 1989.
[30] E.J. Baerends, D. Ellis, P. Ros, Chem. Phys. 2 (1973) 42.
[31] E.J. Baerends P. Ros, Chem. Phys. 2 (1973) 51.
[32] E.J. Baerends, P. Ros, Int. J. Quantum Chem. S12 (1978) 169.
[33] M.S. Gordon, M.T. Carroll, J.H. Jensen, L.P. Davis, L.W. Burgraff, R.M. Guidry, Organometallics 10 (1991) 2657.
[34] M.W. Schmidt, T.L. Windus, M.S. Gordon, J. Am. Chem. Soc. 117 (1995) 7480.
[35] G. Forgács, M. Kolonits, I. Hargittai, Struct. Chem. 1 (1990) 245.
[36] R. McWeeney, Methods of Molecular Quantum Mechanics, Academic Press, London, 2nd edn., 1992.
[37] A. Szabo, N.S. Ostlund, Modern Quantum Chemistry, Introduction to Advanced Electronic Structure Theory. McGraw-Hill, 1989.
[38] J.C. Slater, Quantum Theory of Molecules and Solids, vol. IV, McGraw-Hill, 1979.
[39] R.O. Jones, Rev. Mod. Phys. 61 (1989) 689.
[40] A. Rosa, E.J. Baerends, Inorg. Chem. 32 (1993) 5637.
[41] R. Goc, D. Fiat, J. Magn. Res. 70 (1986) 295.
[42] M.E.N.P.R.A. Silva, A.J.L. Pombeiro, J.J.R. Fraústo da Silva, R. Herrmann, N. Deus, T.J. Castilho, M.F.C.G. Silva, J. Organomet. Chem. 421 (1991) 75.
[43] P.M. Boerrigter, G. te Velde, E.J. Baerends, Int. J. Quantum Chem. 33 (1988) 87.
[44] G. te Velde, E.J. Baerends, J. Comp. Phys. 99 (1992) 84.
[45] R.G. Parr, W. Yang, Density Functional Theory of Atoms and Molecules, Oxford University Press, New York, 1989.
[46] S.H. Vosko, L. Wilk, M. Nusair, Can. J. Phys. 58 (1980) 1200.
[47] H. Stoll, E. Golka, E. Preuss, Theor. Chim. Acta 29 (1980) 55.

[48] Y. Yamaguchi, Y. Osamura, J.D. Goddard, H.F. Schaefer III, A New Dimension to Quantum Chemistry. Analytical Derivative Methods in Ab Initio Molecular Electronic Structure Theory, Oxford University Press, New York, 1994.
[49] R. Hoffmann, J. Chem. Phys. 39 (1963) 1397.
[50] R. Hoffmann, W.N.J. Lipscomb, J. Chem. Phys. 36 (1962) 2179.
[51] R. Hoffmann, W.N.J. Lipscomb, J. Chem. Phys. 36 (1962) 3489.
[52] J.H. Ammeter, H.-B. Bürgi, J.C. Thibeault, R. Hoffmann, J Am. Chem. Soc. 100 (1978) 3686.
[53] C. Mealli, D.M. Proserpio, J. Chem. Ed. 67 (1990) 399.